ELSEVIER

Journal of Alloys and Compounds 408–412 (2006) 313–318

Journal of ALLOYS AND COMPOUNDS

www.elsevier.com/locate/jallcom

Crystal structure and its magnetization of rare earth–iron alloys by mechanical alloying

Hiromasa Yabe [a], Toshiro Kuji [b,*]

[a] *Japan Society for the Promotion of Science, Japan*

[b] *Graduate School of High Technology for Human Welfare, Tokai University, 317 Nishino, Numazu, Shizuoka 410-0395, Japan*

Available online 17 June 2005

Abstract

In this study, binary mixtures of rare earth–iron powders were prepared by mechanical alloying under argon atmosphere. According to the binary equilibrium phase diagram, solubility of rare earth in iron at room temperature is extremely small. This is because of the existence of that bcc iron equilibrates with the extremely stable intermetallic compounds. In this work, it was found that mechanical alloying drastically increased solubility of rare earth in iron, which is much higher than solubility limits estimated from the equilibrium phase diagram. Furthermore, in this study, it was demonstrated that mechanically alloying production of dominant bcc-phase with amorphous phase at room temperature even at relatively high terbium composition. And their magnetization hystereses were gradually broadened with increasing of rare earth atoms. The coercive force values were almost independent of alloy composition. Especially, the coercive force of terbium–iron powders was drastically increased with increasing terbium concentration. It was suggested that the reason of the above behavior was originated by the existence of rare earth atoms in amorphous phases.

Keywords: Tb–Fe; Dy–Fe; Mechanical alloying (MA); Body center cubic (bcc); Coercive force (H_c)

1. Introduction

Recently, syntheses of metastable phases by using mechanical alloying technique have been extensively studied for even immiscible element couples. For example, it has been reported that mechanical alloying of iron–copper mixtures yielded the formation of nanocrystalline solid solutions [1–3]. It can be explained that enthalpy, derived from the energy created by heavy plastic deformation of powders and stress-field dislocations during mechanical alloying, could serve as the driving force for alloying.

In our works, mechanical alloying yields the formation of high temperature bcc-phase by excess energy created during repeated hard plastic deformation of titanium and chromium elements [4]. In addition, it was demonstrated that mechanically alloying yielded formation of single phase of bcc with iron–30 at.% palladium at room temperature [5]. In the past study, it was demonstration that the structures of liquid quenched [6] or sputtered [6–8] iron–palladium alloys formation of dominant fcc phase, which exists at higher temperature for the binary phase diagram.

Rare earth–iron alloys have attracted growing interest as one of the most important magnetic materials, i.e., permanent magnets [9–11], magnetostrictive actuator [12,13], perpendicular magnetic recording media [14,15] and so on. According to binary phase diagrams, solubility of rare earth in iron at room temperature is extremely small. This is because of that bcc iron equilibrates with the existence of the extremely stable intermetallic compounds. Magnetic properties in equilibrated rare earth–iron alloys vary with the different crystal structure with different alloy composition existing in the binary phase diagram. On the other hand, magnetic properties in metastable rare earth–iron alloys change continuously against composition. Continuous changes of magnetic properties with alloy composition can be useful for practical engineering application. Consequently, fundamental properties of amorphous bulk materials [16–18] and sputtered films [19,20] have been previously discussed. These methods were

* Corresponding author. Tel.: +81 55 968 1211x1414; fax: +81 55 968 1224.

E-mail address: tkuji@urchin.fc.u-tokai.ac.jp (T. Kuji).

0925-8388/$ – see front matter © 2005 Elsevier B.V. All rights reserved.
doi:10.1016/j.jallcom.2005.04.056

based upon rapid cooling from high temperature phase to room temperature phase. On the one hand, the formation of metastable phases by mechanical alloying is produced during solid-state reaction.

As mentioned preciously, mechanical alloying has potentially attractive advantages for metallurgists. However, it is difficult to prepare the rare earth–iron alloys by mechanical alloying because rare earth atoms were easily reacted with oxygen. Therefore, the high-energy mechanical alloying apparatus (NEV-MA8, Nissin-Giken, Japan) was selected. This apparatus can be almost ideal for our purpose of mechanical alloying that is continuous water-cooling, keep room temperature of powder and can continuous gas flowing.

In this paper, binary mixture of rare earth (Tb, Dy)–iron powders were prepared by mechanical alloying under argon atmosphere at room temperature, and its fundamental properties, i.e., structure and magnetization were analyzed.

2. Experimental procedure

Elemental powders of Fe (purities 99.9%, <150 μm), Tb (99.9%, <500 μm) and Dy (99.9%, <500 μm) were blended to reach nominal compositions of (a) Tb_8Fe_{92}, (b) $Tb_{16}Fe_{84}$, (c) $Tb_{24}Fe_{76}$, (d) Dy_8Fe_{92}, (e) $Dy_{16}Fe_{84}$ and (f) $Dy_{24}Fe_{76}$, respectively (see Fig. 1 [21]). After pre-mixing the elemental powders to the desired composition, the powder mixture was poured into a stainless steel (SUS304) container together with 1/2 in. diameter stainless steel (SUS304) balls and sealed under an argon atmosphere in a glove box. The mechanical alloying was carried out with keep room temperature for milling duration of 20 h at a speed of 710 rpm. A ball-to-powder weight ratio was 40:1 with 3 g material milled at once. Subsequently to mechanical alloying, the ethanol was pouring into the container to prevent oxidation [22]. After drying, structure and magnetization properties of alloys were analyzed by following equipments.

The phases in the mechanical alloyed powders were identified by X-ray diffraction (XRD) using Cu Kα radiation

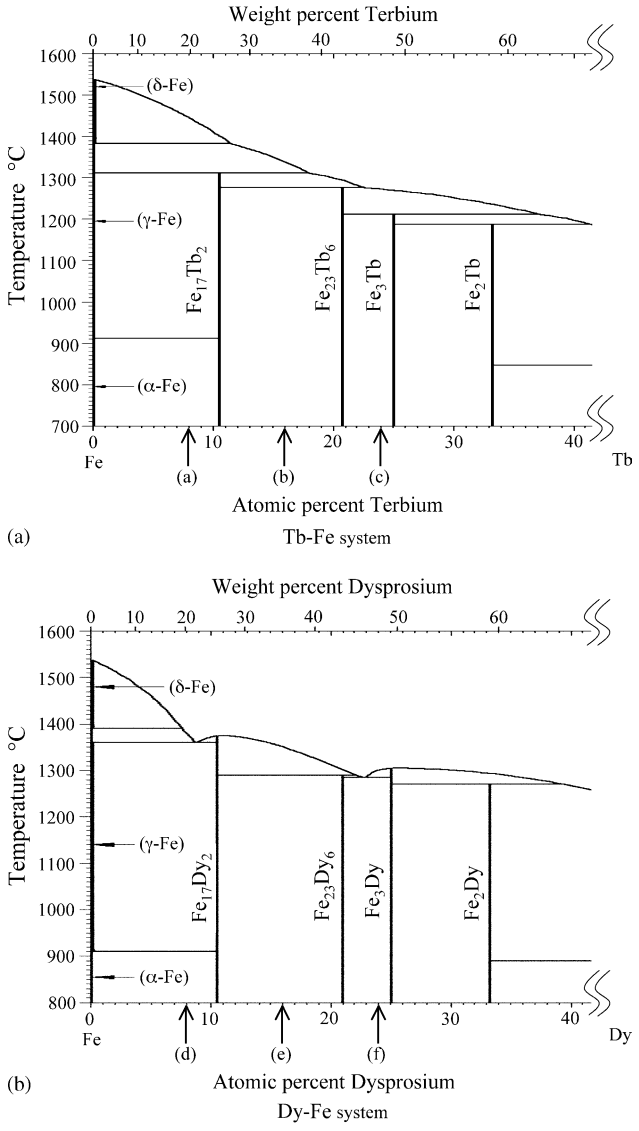

Fig. 1. Tb–Fe and Dy–Fe phase diagrams (from ref. [21]) with nominal compositions.

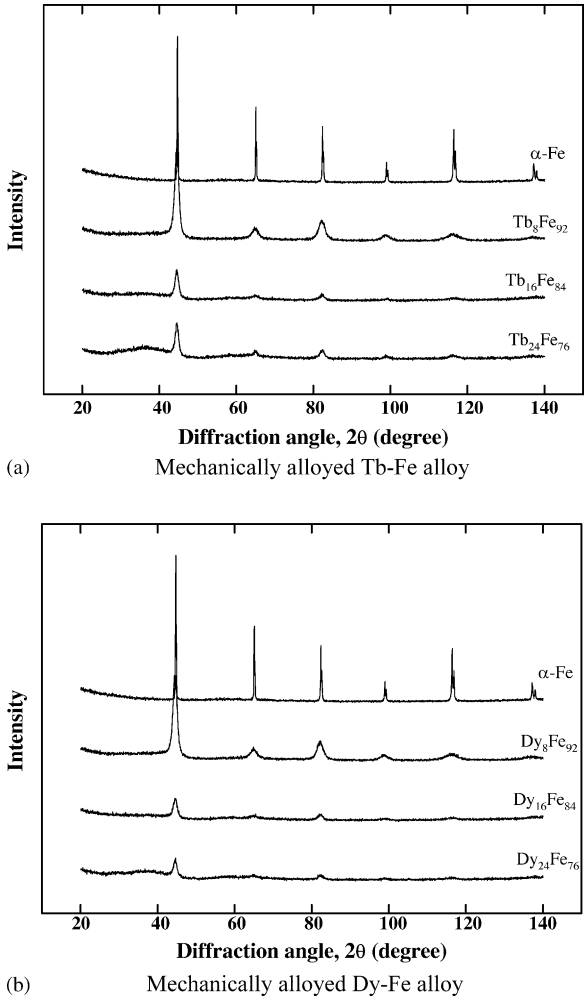

Fig. 2. XRD profiles of synthesized Tb–Fe and Dy–Fe alloys after 20 h of MA.

at room temperature. Anti-reflection silicone was used for the sample holder. The microstructures of the powders were investigated under a scanning electron microscope (SEM). The thermal behaviors of the mechanical alloyed powders were determined by a differential scanning calorimeter (DSC) at a heating rate of 20 K/min in an argon flow atmosphere. The DSC measurements were carried out in a globe box. Magnetic hysteresis measurements were carried out using the vibrating sample magnetomator (VSM) apparatuses combined with an electric magnet with maximum magnetic field of 15 kOe. We used powder sample in plastic capsule with a weight of a few hundred milligrams.

3. Results and discussion

3.1. Structures of synthesized Tb–Fe and Dy–Fe alloys

Fig. 2 shows the powder XRD profiles of synthesized Tb–Fe, Dy–Fe alloys after 20 h of mechanical alloying with diffraction profile of non-treatment α-Fe powder as reference. Diffraction peaks from bcc-phase dominate the XRD patterns over the diffraction scan, suggesting that the elemental powders were well mechanically alloyed. The SEM micrographs (see Fig. 3) also suggest that the initial powders were well mixing only after 20 h of mechanical alloying. For

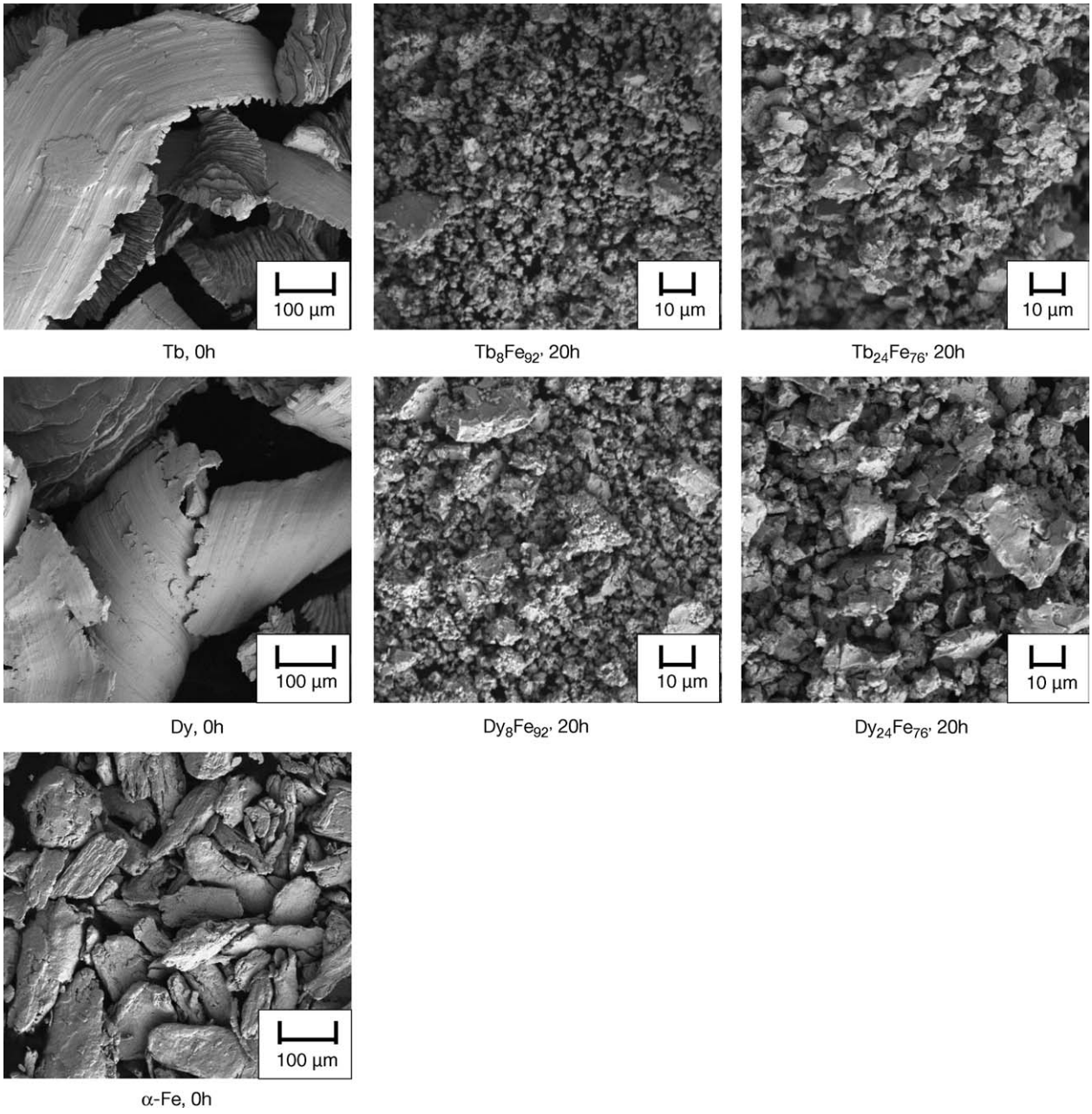

Fig. 3. SEM micrographs of synthesized Tb–Fe and Dy–Fe alloys after 20 h of MA.

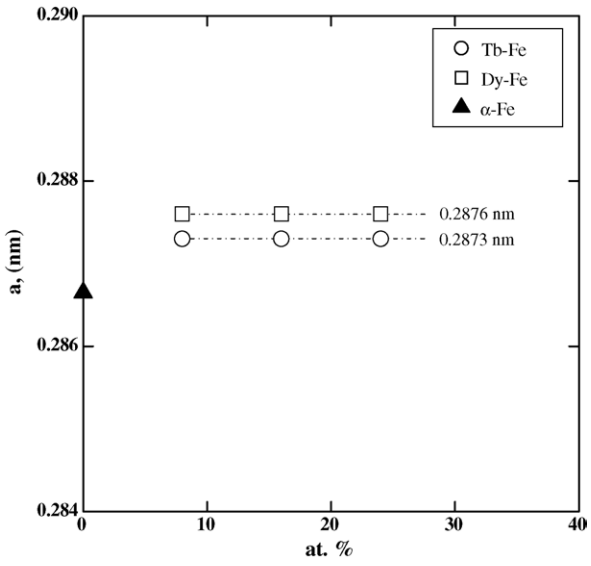

Fig. 4. Lattice parameters *a* from the XRD profiles of mechanically alloyed Tb–Fe and Dy–Fe alloys.

mechanically alloyed Tb–Fe and Dy–Fe powders, the small halo at low diffraction angle of 30–43° should indicate the existence of an amorphous phase in these alloys. Exothermic peak at around 900 K for DSC curves of mechanically alloyed evidently appeared for Tb–Fe and Dy–Fe powders. In the similar experimental results of halos and DSC peaks have been reported for mechanically alloyed samarium–iron powders by Wolf's group [23].

The intensities of the Cu Kα-diffraction peaks of bcc-phase were drastically reduced of each powders with increasing of rare earth atoms. Also bcc-reflections were strongly broadened. The diffraction peaks sift to low angle was observed, although concentration of the rare earth atoms in alloys could be more and less than 8 at.%. The measured lattice parameters *a* and grain size of *D* from the XRD profiles were plotted at Figs. 4 and 5. The lattice parameters of mechanically alloyed Tb–Fe and Dy–Fe powders were around 0.2873 and 0.2876 nm, respectively. The expansion of the bcc-structure lattice suggests the dissolution of rare earth atoms into α-Fe lattice at room temperature. This was reasonably explained with the larger atomic diameters of the terbium and dysprosium atoms than that of the iron atom. From Fig. 4, it can be estimated that amount of rare earth element in the alloys is about 8 at.% and residual rare earth atoms are distributed to amorphous phase indicated by halo

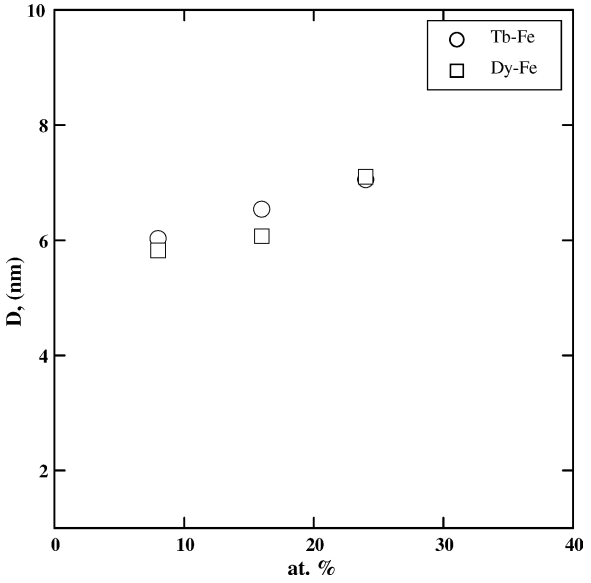

Fig. 5. Grain size, *D* of mechanically alloyed Tb–Fe and Dy–Fe alloys, calculated from XRD peak width.

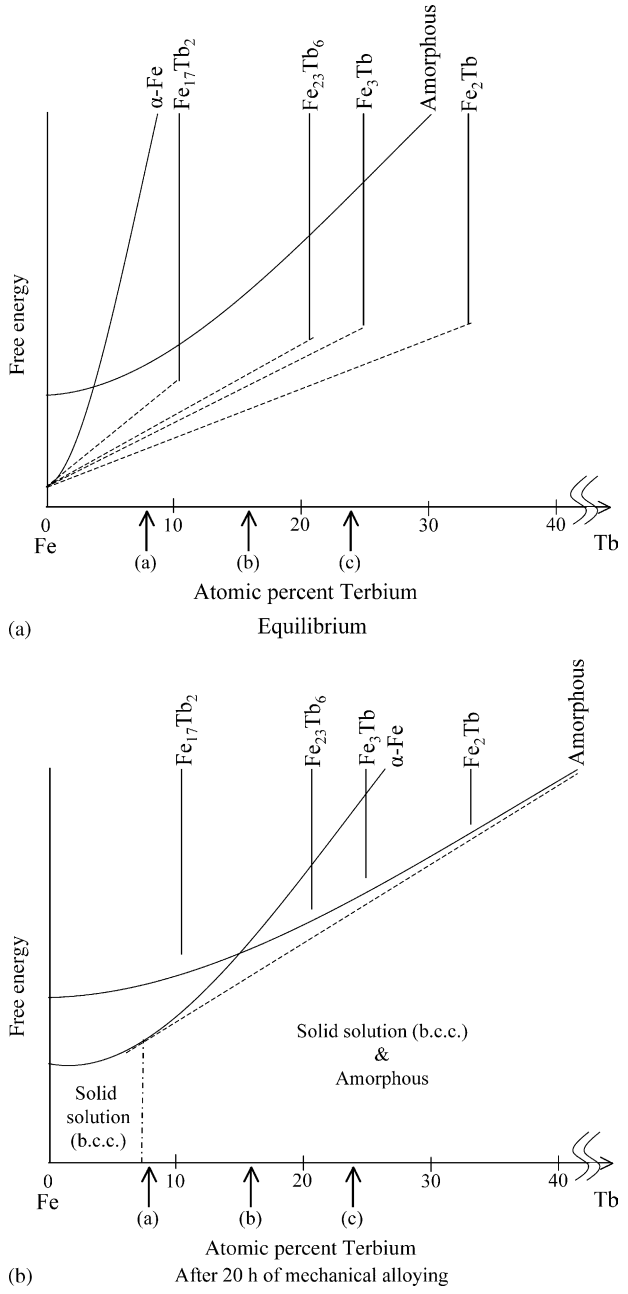

Fig. 6. Schematic illustration of free energy curves. (a) Equilibrium, (b) after 20 h of mechanical alloying

pattern shown in Fig. 2. On the other hand, the grain size value calculated from the XRD peak width using Scherrer's equation, explained that mechanical alloying of rare earth–iron mixture yielded the formation of single nano-sized solid solutions. The lattice image of mechanically alloyed Tb–Fe and Dy–Fe alloys implies that the small amount of amorphous phase coexists with bcc-phase as expected from XRD and DSC results.

According to the binary equilibrium phase diagram, solubility of rare earth in iron at room temperature is very limited, i.e., only few at.%. This is because of the existence of the extremely stable intermetallic compounds. Fig. 6 illustrates free energies expected for α-iron, amorphous iron–terbium alloy and iron–terbium intermetallic compounds, i.e., $Fe_{17}Tb_2$, $Fe_{23}Tb_6$, Fe_3Tb and Fe_2Tb. Fig. 6a shows the equilibrium free energy curves. From the common tangent between iron and imtermettalic compound, the extremely small solubility of terbium in α-iron can be estimated. However, from present experimental results, it was found that mechanical alloying drastically increased solubility of rare earth in α-iron. This behaviour can be understood as follows. The heavy plastic deformation of powders during mechanical alloying creates almost single nano-sized grains as seen in Fig. 5, suggesting that large amount of enthalpy resulted from the plastic deformation might be added to the free energy of α-iron and other phases. Fig. 6b shows the free energy curves after 20 h of mechanical alloying. As seen in Fig. 6b, it can be easily understand that the common tangent demonstrates that mechanically alloying yielded bcc-phase with amorphous phase. And its solubility limit was increased to 8 at.% of rare earth atom at room temperature. In the similar behaviour was expected for iron–dysprosium alloys.

3.2. Magnetization of Tb–Fe and Dy–Fe alloys

Fig. 7 shows the magnetization hysteresis of mechanically alloyed Tb–Fe, Dy–Fe alloys with *M–H* loops of non-treatment α-Fe, terbium and dysprosium powders as

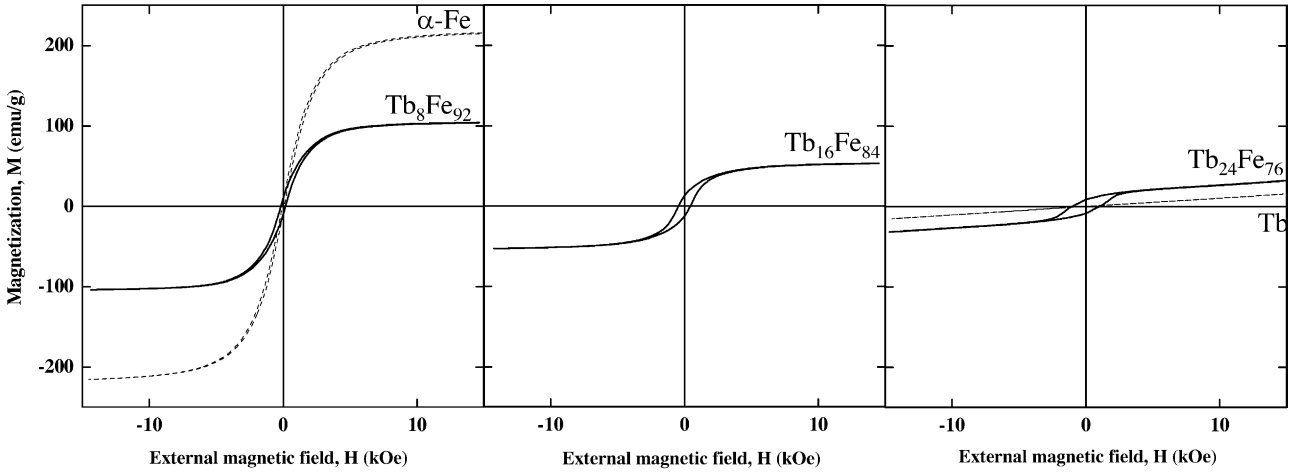

(a) Mechanically alloyed Tb-Fe alloy

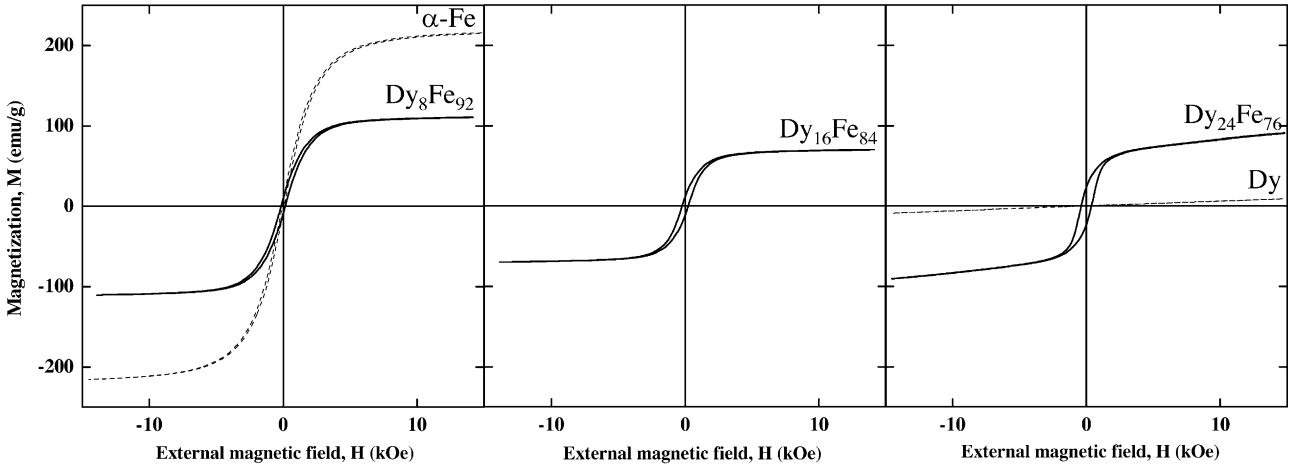

(b) Mechanically alloyed Dy-Fe alloy

Fig. 7. *M–H* loops of mechanically alloyed Tb–Fe and Dy–Fe alloys.

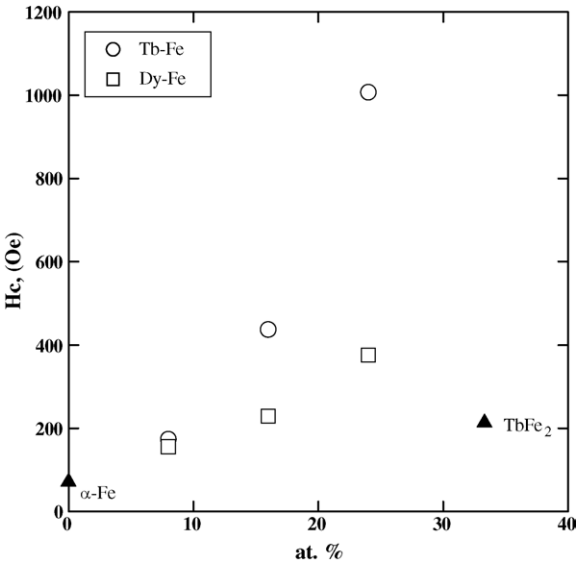

Fig. 8. H_c vs. composition for mechanically alloyed Tb–Fe and Dy–Fe alloys.

reference. The hystereses of the mechanically alloyed powders were gradually broadened with increasing of rare earth atoms. For $Tb_{24}Fe_{76}$ and $Dy_{24}Fe_{76}$ powders, the saturations of magnetizations were not shown at 15 kOe of the external magnetic field. The coercive force H_c is shown in Fig. 8 as functions of compositions. The values of H_c were almost independent of alloy composition. Especially, the coercive force of terbium–iron powders was drastically increased with increasing terbium concentration. In the similar experimental results of behaviours of coercive force have been reported for amorphous rare earth–iron alloys by Miura et al. [24]. From XRD results, it could be expected the solubility limits of terbium or dysprosium in bcc iron are almost 8 at.%, suggesting that the reason of above behavior was originated by existence of rare earth atoms in amorphous phases.

4. Conclusion

Nanocrystalline bcc terbium–iron and dysprosium–iron alloy powders prepared by mechanical alloying based on high power, good argon atmosphere and water-cooling. In this study, fundamental properties of structures and magnetizations were determined. XRD studies revealed that the dissolution of rare earth atoms into α-Fe lattice is about 8 at.% at room temperature and fraction of rare earth atoms are distributed to amorphous. In addition, it should be noticed that mechanical alloying of rare earth–iron mixtures yielded the formation of single nano-sized solid solutions. And their VSM hystereses were gradually broadened with increasing of rare earth atoms. The coercive force values were almost independent of alloy composition. Especially, the coercive force of terbium–iron powders was drastically increased with increasing terbium concentration. It was suggested that the reason of the above behavior was originated by the existence of rare earth atoms in amorphous phases. In order to confirm these results, more precise studies on the structures and magnetic properties at higher or lower temperatures are necessary for many specimens with various different compositions. These features will be reported in near future.

Acknowledgements

T.K. and H.Y. would like to acknowledge for the financial support from Tokyo Ohka Foundation and Tanaka-Kikinzoku Foundation. H.Y. would like to acknowledge for the grant in the Japan Society for the Promotion of Science (JSPS). Mr. Ogawa and Prof. Koizumi, Tokai University are acknowledged for their support in the instrumental VSM analysis.

References

[1] J. Eckert, R. Birringer, J.C. Holzer, C.E. Krill III, W.L. Johnson, Mat. Res. Symp. Proc. 238 (1992) 739.
[2] A.R. Yavari, P.J. Desre, T. Benameur, Phys. Rev. Lett. 68 (2003) 2235.
[3] T. Mashimo, X. Huang, X. Fan, Phys. Rev. B-66 (2002) 132407.
[4] H. Yabe, T. Kuji, J. Alloys Compd., submitted for publication.
[5] H. Yabe, T. Kuji, J. Metastable Nanocryst. Mater., submitted for publication.
[6] H. Yabe, Doctor Thesis in TOKAI University (JAPAN), March 24, 2003, p. 48 (Chapter 4).
[7] H. Yabe, Y. Nishi, Jpn. J. Appl. Phys. 42 (2003) 96.
[8] H. Yabe, Y. Nishi, Tetsu to Hagane 89 (2003) 303.
[9] K. Schnitzke, L. Schultz, C. Kuhrt, L. Schultz, M. Katter, Appl. Phys. Lett. 57 (1990) 2853.
[10] M. Endoh, M. Iwata, M. Tokunaga, J. Appl. Phys. 70 (1991) 6030.
[11] C.N. Chistodoulou, T. Takeshita, J. Alloys Compd. 196 (1993) 161.
[12] E. Quandt, J. Alloys Compd. 258 (1997) 126.
[13] H. Wakiwaka, K. Aoki, T. Yoshikawa, M. Igarashi, H. Yamada, J. Alloys Compd. 258 (1997) 87.
[14] K. Kojima, M. Hamamoto, J. Sato, K. Watanabe, H. Katayama, IEEE Trans. Magn. 37 (2001) 1406.
[15] Y.G. Ma, Z. Yang, M. Matsumoto, A. Morisako, S. Takei, J. Magn. Magn. Mater. 267 (2003) 341.
[16] T. Harada, T. Kuji, K. Fukuoka, Y. Syono, J. Mater. Sci. Lett. 11 (1992) 1072.
[17] T. Harada, T. Kuji, K. Fukuoka, Y. Syono, J. Alloys Compd. 191 (1993) 255.
[18] T. Harada, M. Fujita, T. Kuji, J. Alloys Compd. 243 (1996) 139.
[19] H. Uchida, Y. Matsumura, H-H. Uchida, H. Kaneko, J. Magn. Magn. Mater. 239 (2002) 540.
[20] M. Takeuchi, Y. Matsumura, H. Uchida, T. Kuji, Mat. Trans. JIM 45 (2004) 225.
[21] Binary phase diagram, ASM International.
[22] H. Nakano, T. Kuji, S. Nakayama, J. Mat. Sci. Soc. Jpn. 41 (2004) 32.
[23] A. Teresiak, M. Kubis, N. Mattern, M. Wolf, K.-H. Muller, J. Alloys Compd. 274 (1998) 284.
[24] Y. Miura, N. Imamura, T. Kobayashi, A. Okada, Y. Kushiro, J. Appl. Phys. 49 (1978) 1208.